ISPACS 2006

2006 International Symposium on Intelligent Signal Processing and Communication Systems (ISPACS2006)
Yonago Convention Center, Tottori, Japan

A Dental Radiograph Registration Algorithm Using Phase-Based Image Matching for Human Identification

Akira Nikaido, Koichi Ito, Takafumi Aoki
Graduate School of Information Sciences,
Tohoku University,
Sendai 980–8579, Japan
E-mail: {nikaido, ito}@aoki.ecei.tohoku.ac.jp

Eiko Kosuge, Ryota Kawamata
Department of Oral and Maxillofacial Radiology,
Kanagawa Dental College,
82, Inaoka, Yokosuka, 238-8580 Japan

***Abstract*— Dental records are often used to identify victims of massive disasters, where the conventional biometric features, e.g., face, fingerprint, iris, etc., are not available. Human identification using dental records is to match an unidentified individual's postmortem radiographs against a set of identified antemortem radiographs. This paper presents an efficient dental radiograph registration algorithm using phase-based image matching for human identification. The use of phase components in 2D (two-dimensional) discrete Fourier transforms of dental radiograph images makes possible to achieve highly robust image registration and recognition. Experimental evaluation using a small database of dental radiographs indicates that the proposed algorithm exhibits efficient recognition performance for low-quality images.**

I. Introduction

Biometric authentication has been playing an important role in identifying individuals using their physiological and behavioral characteristics such as face, fingerprint, iris, etc. On the other hand, when identifying victims of large-scale disasters, e.g., earthquake, fire disaster, tsunami, etc., the conventional biometric traits may not be available. Addressing this problem, dental records have been used in identifying deceased individuals.

Human identification using dental radiographs, which is called dental biometrics, is to match an unidentified individual's postmortem (PM) radiographs against a set of identified antemortem (AM) radiographs. Figure 1 shows an example of dental radiograph, which is a periapical image around molars. In forensic odontology, which is also called forensic dentistry, a one-by-one comparison between the AM and PM radiographs is done manually by forensic experts. Since this task is extremely time consuming, the demand for the automated dental identification system has increased [1].

Previous works of the automated dental radiograph identification use the contours of the teeth and the shapes of the dental work to compare between the AM and PM dental images [1], [2], [3]. One of the difficult problems in feature-based approach is that the matching performance is significantly influenced by the image quality of radiographs. In many cases, the contours of the teeth can not be extracted from the dental radiograph correctly, since the dental radiograph is often blurred due to substantial noise, poor lighting, etc.

Fig. 1. Example of dental radiograph, which is a periapical image around molars.

This paper presents an efficient algorithm for dental radiograph image registration using phase-based image matching — an image matching technique using the phase components in 2D Discrete Fourier Transforms (DFTs) of given images. The technique has been successfully applied to sub-pixel image registration tasks for computer vision applications [4], [5], [6].

In our previous work [7], we have proposed a fingerprint recognition algorithm using phase-based image matching, which has already been implemented in actual fingerprint verification units [8]. We also have proposed iris recognition [9] and palmprint recognition [10] algorithms using phase-based image matching.

In this paper, we demonstrate that the same technique is also highly effective for dental biometrics. Experimental evaluation using a set of dental radiographs taken before and after dental treatment demonstrates efficient registration performance of the proposed algorithm.

II. Phase-Based Image Matching

A. POC function

We introduce the principle of phase-based image matching using the Phase-Only Correlation (POC) function (which is sometimes called the "phase-correlation function") [4], [5], [6].

0-7803-9733-9/06/$20.00©2006 IEEE

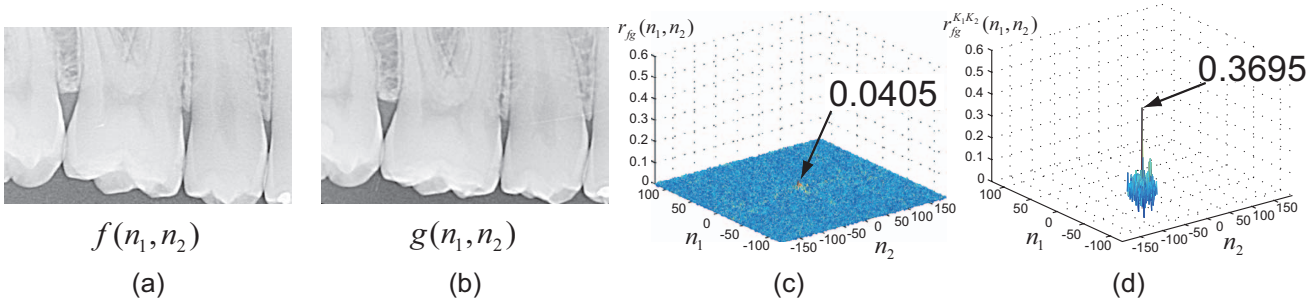

Fig. 2. Example of image matching using the original POC function and the BLPOC function: (a) reference image $f(n_1, n_2)$, (b) input image $g(n_1, n_2)$, (c) original POC function $r_{fg}(n_1, n_2)$ and (d) BLPOC function $r_{fg}^{K_1K_2}(n_1, n_2)$ with $K_1/M_1 = 0.1$ and $K_2/M_2 = 0.1$.

Consider two $N_1 \times N_2$ images, $f(n_1, n_2)$ and $g(n_1, n_2)$, where we assume that the index ranges are $n_1 = -M_1, \cdots, M_1$ ($M_1 > 0$) and $n_2 = -M_2, \cdots, M_2$ ($M_2 > 0$) for mathematical simplicity, and hence $N_1 = 2M_1 + 1$ and $N_2 = 2M_2 + 1$. Let $F(k_1, k_2)$ and $G(k_1, k_2)$ denote the 2D DFTs of the two images. $F(k_1, k_2)$ is given by

$$\begin{aligned} F(k_1, k_2) &= \sum_{n_1, n_2} f(n_1, n_2) W_{N_1}^{k_1 n_1} W_{N_2}^{k_2 n_2} \\ &= A_F(k_1, k_2) e^{j\theta_F(k_1, k_2)}, \end{aligned} \tag{1}$$

where $k_1 = -M_1, \cdots, M_1$, $k_2 = -M_2, \cdots, M_2$, $W_{N_1} = e^{-j\frac{2\pi}{N_1}}$, $W_{N_2} = e^{-j\frac{2\pi}{N_2}}$, and $\sum_{n_1, n_2}$ denotes $\sum_{n_1=-M_1}^{M_1} \sum_{n_2=-M_2}^{M_2}$. $A_F(k_1, k_2)$ is amplitude and $\theta_F(k_1, k_2)$ is phase. $G(k_1, k_2)$ is defined in the same way. The cross-phase spectrum $R_{FG}(k_1, k_2)$ is given by

$$R_{FG}(k_1, k_2) = \frac{F(k_1, k_2)\overline{G(k_1, k_2)}}{|F(k_1, k_2)\overline{G(k_1, k_2)}|} = e^{j\theta(k_1, k_2)}, \tag{2}$$

where $\overline{G(k_1, k_2)}$ is the complex conjugate of $G(k_1, k_2)$ and $\theta(k_1, k_2)$ denotes the phase difference $\theta_F(k_1, k_2) - \theta_G(k_1, k_2)$. The POC function $r_{fg}(n_1, n_2)$ is the 2D Inverse DFT (2D IDFT) of $R_{FG}(k_1, k_2)$ and is given by

$$r_{fg}(n_1, n_2) = \frac{1}{N_1 N_2} \sum_{k_1, k_2} R_{FG}(k_1, k_2) W_{N_1}^{-k_1 n_1} W_{N_2}^{-k_2 n_2}, \tag{3}$$

where $\sum_{k_1, k_2}$ denotes $\sum_{k_1=-M_1}^{M_1} \sum_{k_2=-M_2}^{M_2}$. When two images are similar, their POC function gives a distinct sharp peak. When two images are not similar, the peak drops significantly. The height of the peak gives a good similarity measure for image matching, and the location of the peak shows the translational displacement between the images.

B. Band-limited POC function

We modify the definition of POC function to have a BLPOC (Band-Limited Phase-Only Correlation) function [7] dedicated to biometric authentication task. The idea to improve the matching performance is to eliminate meaningless high frequency components in the calculation of cross-phase spectrum R_{FG} depending on the inherent frequency components of images. Assume that the ranges of the inherent frequency band are given by $k_1 = -K_1, \cdots, K_1$ and $k_2 = -K_2, \cdots, K_2$, where $0 \le K_1 \le M_1$ and $0 \le K_2 \le M_2$. Thus, the effective size of frequency spectrum is given by $L_1 = 2K_1 + 1$ and $L_2 = 2K_2 + 1$. The BLPOC function is given by

$$r_{fg}^{K_1K_2}(n_1, n_2) = \frac{1}{L_1 L_2} {\sum_{k_1, k_2}}' R_{FG}(k_1, k_2) W_{L_1}^{-k_1 n_1} W_{L_2}^{-k_2 n_2}, \tag{4}$$

where $n_1 = -K_1, \cdots, K_1$, $n_2 = -K_2, \cdots, K_2$, and $\sum'_{k_1, k_2}$ denotes $\sum_{k_1=-K_1}^{K_1} \sum_{k_2=-K_2}^{K_2}$. Note that the maximum value of the correlation peak of the BLPOC function is always normalized to 1 and does not depend on L_1 and L_2.

Figure 2 shows an example of genuine matching using the original POC function r_{fg} and the BLPOC function $r_{fg}^{K_1K_2}$. The BLPOC function provides the higher correlation peak and better discrimination capability than that of the original POC function.

C. Rotation angle estimation

The phase-based image matching technique mentioned above can be extended to the registration for images including translation, rotation and scaling simultaneously [5]. In this paper, we focus on the rotation alignment using the phase-based image matching. We employ the polar mapping of the amplitude spectrum to transform the image rotation into image translation. The rotation angle is estimated by detecting the corresponding translational displacements by the above technique. We summarize the procedure for estimating the rotation angle θ as follows (see [5] for detailed discussions).

1) Calculate 2D DFTs of $f(n_1, n_2)$ and $g(n_1, n_2)$ to obtain $F(k_1, k_2)$ and $G(k_1, k_2)$.
2) Calculate amplitude spectra $|F(k_1, k_2)|$ and $|G(k_1, k_2)|$ (Fig. 3 (b)). In general, most energy is concentrated in low-frequency domain. Hence, we use $\sqrt{|F(k_1, k_2)|}$ and $\sqrt{|G(k_1, k_2)|}$ in stead of $|F(k_1, k_2)|$ and $|G(k_1, k_2)|$ (Fig. 3 (c)).
3) Calculate the polar mappings $|F_P(l_1, l_2)|$ and $|G_P(l_1, l_2)|$ (Fig. 3 (d)).
4) Estimate the image displacement between $|F_P(l_1, l_2)|$ and $|G_P(l_1, l_2)|$ using the peak location of the BLPOC function $r_{|F_P||G_P|}^{K_1K_2}(n_1, n_2)$ to obtain θ.

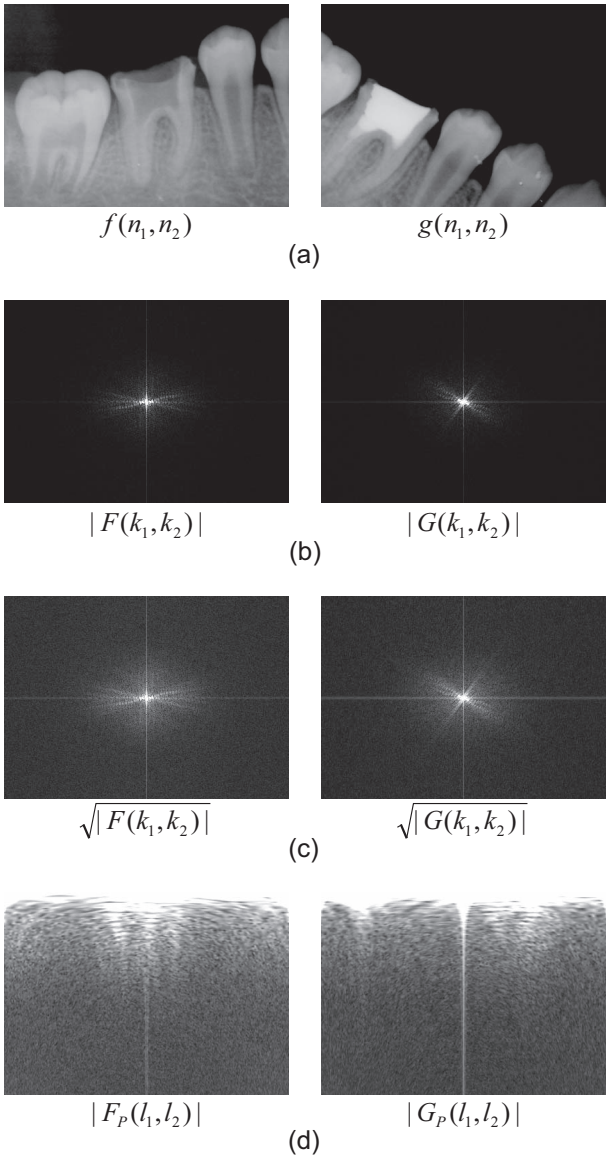

Fig. 3. Rotation angle estimation using phase-based image matching: (a) the registered image and the input image, (b) amplitude spectra of the images, (c) square root of the amplitude spectra, and (d) polar mappings of the amplitude.

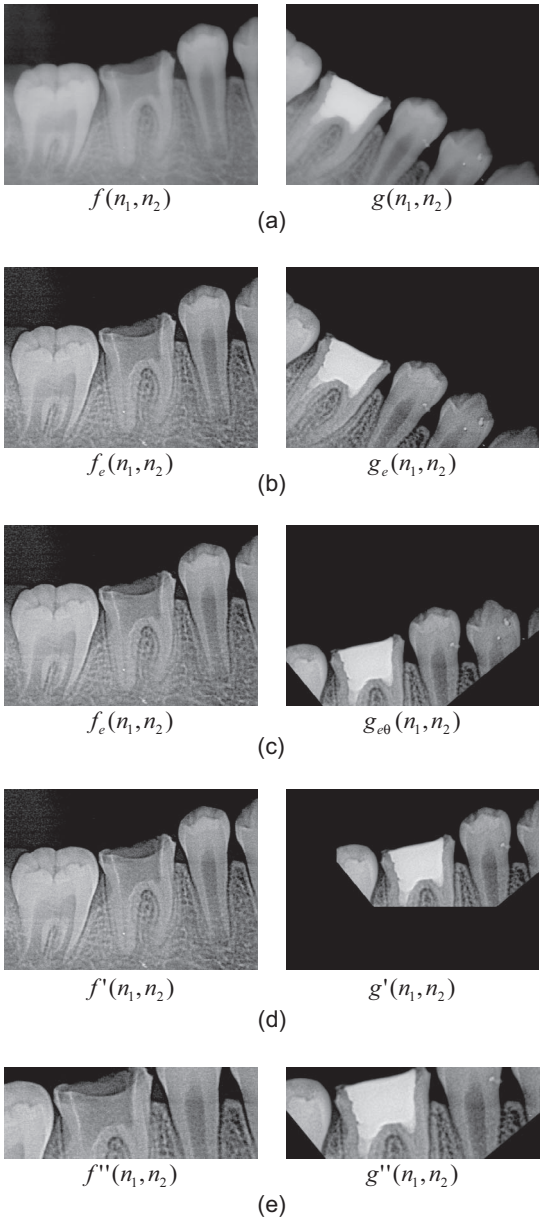

Fig. 4. Example of dental radiograph registration and matching using the proposed algorithm: (a) the registered image and the input image, (b) enhanced images, (c) rotation-normalized images, (d) normalized images, and (e) extracted common regions.

III. Dental Registration Algorithm

In this section, we present a dental registration algorithm using the POC function. The proposed algorithm consists of the four steps: (i) image enhancement, (ii) rotation and displacement alignment, (iii) common region extraction and (iv) dental matching. Steps (iii) and (iv) are for evaluating the registration performance.

(i) Image enhancement

First step is the enhancement of radiograph image to allow accurate radiograph image processing, since these images are often blurred due to substantial noise, poor lighting, etc. In our proposed algorithm, we improve the image quality by using local area contrast enhancement [11]. Figure 4 (b) shows the enhanced images, $f_e(n_1, n_2)$ and $g_e(n_1, n_2)$, of the registered image $f(n_1, n_2)$ and the input image $g(n_1, n_2)$, respectively.

(ii) Rotation and displacement alignment

We need to normalize rotation and displacement between $f_e(n_1, n_2)$ and $g_e(n_1, n_2)$ in order to perform the high-accuracy dental radiograph matching. We estimate the rotation angle θ by using the technique described in Sect. II-C. Using θ, we obtain a rotation-normalized image $g_{e\theta}(n_1, n_2)$ (Fig. 4 (c)). Then, we align the translational displacement between $f_e(n_1, n_2)$ and $g_{e\theta}(n_1, n_2)$ using the peak location of the BLPOC function $r^{K_1 K_2}_{f_e g_{e\theta}}(n_1, n_2)$, where $K_1/M_1 = K_2/M_2 = 0.5$. Thus, we have normalized versions of the registered image and the input image as shown in Fig. 4 (d), which are denoted

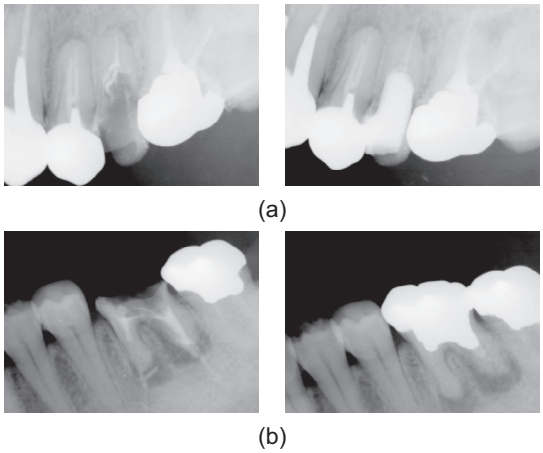

Fig. 5. Examples of dental radiographs in our database: the left-hand images are taken before dental treatment and the right-hand images are taken after dental treatment.

by $f'(n_1, n_2)$ and $g'(n_1, n_2)$.

(iii) Common region extraction

Next step is to extract the overlapped region (intersection) of the two images $f'(n_1, n_2)$ and $g'(n_1, n_2)$. This process improves the accuracy of dental matching, since the non-overlapped areas of the two images become the uncorrelated noise components in the BLPOC function. In order to detect the effective areas in the registered image $f'(n_1, n_2)$ and the input image $g'(n_1, n_2)$, we examine the n_1-axis projection and the n_2-axis projection of pixel values. Only the common effective image areas, $f''(n_1, n_2)$ and $g''(n_1, n_2)$, with the same size are extracted for the succeeding image matching step (Fig. 4 (e)).

(iv) Matching

We calculate the BLPOC function $r^{K_1 K_2}_{f''g''}(n_1, n_2)$ between the two extracted images $f''(n_1, n_2)$ and $g''(n_1, n_2)$, and evaluate the matching score, where $K_1/M_1 = K_2/M_2 = 0.1$. The matching score is the highest peak value of the BLPOC function $r^{K_1 K_2}_{f''g''}(n_1, n_2)$.

IV. Experiment

This section describes a set of experiments using the dental radiograph database for evaluating dental matching performance of the proposed algorithm.

In this experiment, we use dental radiographs taken before and after dental treatment in stead of AM and PM radiographs. Our database consists of 50 images (367×485 pixels) with 25 subjects and 2 different images of each dental radiograph. Figure 5 shows some examples of the dental radiographs in this database.

The registration performance of the proposed algorithm is evaluated by identifying the subjects in order to perform the quantitative evaluation. In this experiment, 25 subjects after dental treatment are matched to the 25 subjects before dental treatment. Figure 6 shows the cumulative match curve of the proposed algorithm, which is sometimes used for evaluating the performance of the identification system. Using the top-1 radiograph, the recognition accuracy is 80% (=20/25). The recognition accuracy reaches 100 % when the top-5 radiographs are used. As is observed in this experimental result, the proposed algorithm is useful for matching low-quality dental radiographs.

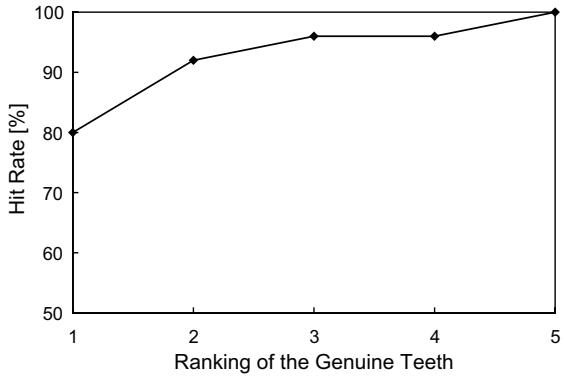

Fig. 6. Cumulative match curve of the proposed algorithm.

V. Conclusion

This paper proposed a dental radiograph registration algorithm using the phase-based image matching. Experimental performance evaluation demonstrates efficient performance of our proposed algorithm for low-quality dental radiographs. For our future work, we aim to develop a dental identification system using phase-based image matching and evaluate the performance of the developed system using large-scale database of AM and PM dental radiographs.

References

[1] G. Fahmy, D. Nassar, E. Haj-Said, H. Chen, O. Nomir, J. Zhou, R. Howell, H. H. Ammar, M. Abdel-Mottaleb, and A. K. Jain, "Toward an automated dental identification system," *J. of Electronic Imaging*, vol. 14, no. 4, pp. 043 018–1–043 018–13, Oct. 2005.

[2] A. K. Jain and H. Chen, "Matching of dental X-ray images for human identification," *Pattern Recognition*, vol. 37, no. 7, pp. 1519–1532, July 2004.

[3] H. Chen and A. K. Jain, "Dental biometrics: Alignment and matching of dental radipgraphs," *IEEE Trans. Pattern Anal. Machine Intell.*, vol. 27, no. 8, pp. 1319–1326, Aug. 2005.

[4] C. D. Kuglin and D. C. Hines, "The phase correlation image alignment method," *Proc. Int. Conf. Cybernetics and Society*, pp. 163–165, 1975.

[5] K. Takita, T. Aoki, Y. Sasaki, T. Higuchi, and K. Kobayashi, "High-accuracy subpixel image registration based on phase-only correlation," *IEICE Trans. Fundamentals*, vol. E86-A, no. 8, pp. 1925–1934, Aug. 2003.

[6] K. Takita, M. A. Muquit, T. Aoki, and T. Higuchi, "A sub-pixel correspondence search technique for computer vision applications," *IEICE Trans. Fundamentals*, vol. E87-A, no. 8, pp. 1913–1923, Aug. 2004.

[7] K. Ito, H. Nakajima, K. Kobayashi, T. Aoki, and T. Higuchi, "A fingerprint matching algorithm using phase-only correlation," *IEICE Trans. Fundamentals*, vol. E87-A, no. 3, pp. 682–691, Mar. 2004.

[8] Products using phase-based image matching. [Online]. Available: http://www.aoki.ecei.tohoku.ac.jp/research/poc.html

[9] K. Miyazawa, K. Ito, , T. Aoki, K. Kobayashi, and H. Nakajima, "A phase-based iris recognition algorithm," *Lecture Notes in Computer Science (ICB2006)*, vol. 3832, pp. 356–365, Dec. 2005.

[10] K. Ito, T. Aoki, H. Nakajima, K. Kobayashi, and T. Higuchi, "A palmprint recognition algorithm using phase-based image matching," *Proc. the 2006 IEEE Int. Conf. Image Processing*, Oct. 2006 (to be published).

[11] G. X. Ritter and J. N. Wilson, *Handbook of Computer Vision Algorithms in Image Algebra*. CRC Press, 1996.